Macromolecular Chemistry and Physics
www.mcp-journal.de

Nonlinear Melt Rheology of Lamellae Forming Polystyrene-*b*-Poly-2-Vinylpyridine Diblock Copolymers

*Matthias Heck and Manfred Wilhelm**

Lamellae forming polystyrene-*b*-poly-2-vinylpyridine diblock copolymer melts are investigated with linear shear rheology and Fourier transformation rheology (FT rheology) to quantify their nonlinear behavior under oscillatory shear via mechanical higher harmonic contributions such as $I_{3/1}(\omega_1, \gamma_0)$. The determination of the zero-shear nonlinearity $({}^3Q_0(\omega) \equiv \lim_{\gamma_0 \to 0} I_{3/1}/\gamma_0^2)$ by a variation of γ_0 is hindered by the increasing domain alignment at increasing γ_0. Thus, an approach for determining ${}^3Q_0(T)$ by a variation of the temperature is developed and used. This approach allows obtaining insights on the nonlinear behavior directly at temperature-dependent phase transitions, such as at the order-disorder transition temperature T_{ODT} of block copolymers. The maximum of ${}^3Q_0$ is found to be close to T_{ODT}. The nonlinearity originating from the connection of the unequal polymer blocks is shown to dominate the overall nonlinearity, and the maximum of ${}^3Q_0(T)$ correlates to domain alignment for $T < T_{ODT}$.

1. Introduction

Block copolymers have emerged over decades as a topic of contemporary macromolecular science and engineering.[1] Block copolymers generate periodic structures in the nanoscale, which can be aligned to obtain macroscopically aniotropic materials and result in unique features.[2,3] For many industrial applications, polymeric materials are processed in the nonlinear mechanical area and thus studies in the nonlinear mechanical regime are of fundamental scientific interest, but may also assist in the processing of these materials. One method for applying mechanical nonlinearity for viscoelastic materials in shear is the application of large amplitude oscillatory shear (LAOS). Oscillatory shear tests result in a wide range of mechanical responses by independently varying the excitation frequency $\omega_1/2\pi$, strain amplitude γ_0, and temperature T.[4] Fourier transformation of the torque in rheology provides the ability to convert the raw stress-time data from oscillatory shear into a frequency spectrum, where the higher harmonics of the excitation frequency can be identified and quantified. Higher harmonic intensities have been used to analyze complex fluids.[5–9]

Under medium and large amplitude oscillatory shear (MAOS and LAOS) the intensity of the higher harmonics changes as a function of the strain amplitude γ_0 and the excitation frequency $\omega_1/2\pi$, with nonlinear mechanical behavior leading to an increase in the odd harmonic of the shear stress at $3\omega_1/2\pi$, $5\omega_1/2\pi$, etc. In several publications, the intensity of the third harmonic I_3 was chosen as a measure to quantify nonlinearity, because it has the largest contribution to the overall nonlinearity (i.e., highest intensity), and thus it has the smallest experimental error.

According to general theories,[10,11] the ratio of the third to the first intensity $I_{3/1}$ is proportional to γ_0^2 at low strain amplitudes. Dynamic strain sweep experiments and also simulations support this assumption, and a scaling exponent of 2, i.e., $I_{3/1} \propto \gamma_0^2$, can be found for $I_{3/1}$ at medium strain amplitudes γ_0 (MAOS).

The intrinsic nonlinearity ${}^3Q_0(\omega)$, as defined by Hyun et al.,[12,13] is a function of the excitation frequency $(\omega_1/2\pi)$.

With the time-temperature superposition (TTS) principle,[14] it was possible to generate "nonlinear master curves" for ${}^3Q_0(\omega)$, using the shift parameters from the respective linear master curves.[15] It was shown that these nonlinear master curves are sensitive to the molecular topology of homopolymers and the topological influence on relaxation processes could be further explained.[13,16–19] The general evolution of ${}^3Q_0(\omega)$ in nonlinear master curves of linear homopolymers follows an increase with frequency or the Deborah number De, respectively, $({}^3Q_0 \propto De^2)$ toward a maximum at $De \approx 1$. For a further increase in frequency, the intrinsic nonlinearity decreases with a lower slope $({}^3Q_0 \propto De^{0.38})$.[15] Taking additional relaxation processes into account, ${}^3Q_0$ exhibits local maxima at frequencies related to these relaxations.[20,21] For complex topologies with a large difference in the longest relaxation time of the components, well-separated maxima of ${}^3Q_0$ can be observed.[22] Although there are investigations of block copolymer melts in the nonlinear regime, i.e., kinetic studies on domain alignment,[23–26] to the best of our knowledge, there is no work on the relaxation processes described by nonlinear master curves. In accord with the nonlinear master curves of complex topologies, nonlinear master curves for block

M. Heck, M. Wilhelm
Institute for Chemical Technology and Polymer Chemistry
Karlsruhe Institute of Technology
76131 Karlsruhe, Germany
E-mail: Manfred.Wilhelm@kit.edu

The ORCID identification number(s) for the author(s) of this article can be found under https://doi.org/10.1002/macp.202300441

DOI: 10.1002/macp.202300441

copolymers with several maxima of ${}^3Q_0$ are conceivable. However, for block copolymer melts, the situation differs from one in which two components of the same type are linked together. Two homopolymer blocks of different polymer types connected to each other by a covalent bond can phase separate and form different domains of different morphologies depending on the volume fraction Φ of the respective polymer block.[27,28] These domains are on the length scale of 1–100 nm. The strength of phase separation depends on χN, the product of the Flory-Huggins parameter χ and the total degree of polymerization N.[29,30] The Flory-Huggins parameter is fixed for a specific pair of monomers and temperature. The parameter χ reflects the difference in their chemical nature and is inversely dependent on temperature T in the general form of $\chi = a + b/T$. If a threshold of χN is reached (i.e., $\chi N = 10.5$ for linear diblock copolymers) the system starts to phase separate.[31] This reversible phase separation can be observed rheologically, by differential scanning calorimetry or by X-ray scattering at the so-called order–disorder transition temperature T_{ODT}, that is generally above the higher glass transition temperature of both components.[32]

Randomly oriented domains, which may be overall microscopically anisotropic, nevertheless form macroscopically isotropic materials. However, these domains can be aligned by external fields, such as electrical fields,[33–38] magnetic[39–41] or mechanical fields,[42–46] just to mention some, to form an anisotropic material on a macroscopic length scale. The superposition of phase separation, domain alignment and molecular stretch and orientation are thus challenges in the determination of the nonlinear behavior of BCP melts, because the domains in the BCP melt are aligned during one measurement (especially at large γ_0) or in between measurements, which obviously influences the obtained results. In this study, lamellae forming polystyrene-*b*-poly(2-vinylpyridine) (PS-*b*-P2VP) diblock copolymers are investigated as a model system for phase separating polymer melts toward their nonlinear mechanical response. This diblock copolymer system was chosen as a model system for reasons of simplicity (i.e., only two polymer blocks and thus no bridges or loops between neighboring domains,[26,47] no difference between internal and terminal polymer blocks and a possible influence,[26] no (flow induced) crystallinity, which would represent an additional time dependent influence parameter.[46]) and suitability for rheological experiments in the melt and morphological characterization (i.e., thermal stability in the melt, sufficient difference in electron density for morphological characterization with small angle X-ray scattering, order disorder transition temperature in an accessible temperature range).[48] The entanglement molecular weight M_e of the polymer blocks ($M_{e,\,PS} = 16.8$ kg mol^{-1} and $M_{e,\,P2VP} = 24.3$ kg mol^{-1}) in combination with a Flory Huggins parameter of $\chi \approx 0.1$, yields non entangled samples with an accessible T_{ODT} and samples with entangled polymer chains, yet no accessible T_{ODT}.[15,49] The comparison of their nonlinear master curves could help to separate the influence of the polymer chain and the phase boundary on ${}^3Q_0$ from each other and thus help to gain insights on the origin of the intrinsic nonlinearity in BCP melts. A direct way to measure and construct nonlinear master curves for BCP melts was developed. The nonlinear regime of the melts was first determined by probing dynamic strain sweep experiments. Experiments in the nonlinear regime while varying the temperature T enabled the construction of nonlinear master curves for BCP melts. The intrinsic nonlinearity above T_{ODT} increased toward the phase transition. Below T_{ODT}, the nonlinearity is influenced by domain alignment by oscillatory shear. The nonlinearity is finally correlated with the interface between the two polymer parts and polymer chains of one type in the lamellae of the other polymer type.

2. Experimental Section

2.1. Methods and Materials

The diblock copolymer was synthesized using anionic polymerization. Thus, high vacuum techniques were used, as described in more detail elsewhere in the literature.[50,51] All glassware was heated to approximately 600 °C and flushed with argon in order to remove all traces of adsorbed water. Reagents were added through a syringe under argon counter flow.

Tetrahydrofurane (THF) (≥99.5 %, Carl Roth) was refluxed over calcium hydride for several days. It was further purified with sodium and benzophenone where a purple color indicated that all traces of water were removed from the solvent. The storage flask was directly connected to the vacuum line, and thus the solvent was removed without contamination. Just before use, the THF was distilled into the reaction flask. Toluene (≥99 %, Fisher) was purified by the addition of secondary butyllithium and 1,1-diphenylethylene and a subsequent distillation. The absence of protic impurities prior to distillation was indicated by a red color of the solution. Secondary butyllithium (sec-BuLi) (1.4 mol l^{-1} in hexane, Sigma–Aldrich) and calcium hydride (CaH_2) were used as received. 1,1-Diphenylethylene (DPE, 98 %, Alfa Aesar) was purified by the addition of n-butyllithium until a dark red color persisted. Diphenylethylene was distilled under high vacuum at 85 °C. Subsequently THF was added to achieve a concentration suitable for the synthesis of the polymer samples. Styrene (99 %, Fisher Scientific) was stirred over CaH_2 for several days and distilled under reduced pressure into an ampule and either used directly or stored at −18 °C for up to two weeks. 2-Vinylpyridine (97 %, Fisher Scientific) was stirred over CaH_2 for several day and distilled under reduced pressure into an ampule as styrene, but used directly. Methanol (≥98.5 %, VWR Chemicals), which was used for the termination of the polymerization reactions, was frozen with liquid nitrogen and subsequently thawed to remove oxygen and prevent coupling of two macro anions leading to a doubling of the molecular weight. This procedure was repeated until no more gas bubbles were observed.

2.2. Synthesis

Two slightly different synthetic routes were used for the synthesis of the PS-*b*-P2VP samples used in this study, which are displayed in **Figure 1**. In route 1, the reactivity of the macro anions was kept low in order to have the most control over the polymerization reaction and decrease the possibility of side reactions. The reactivity adaption was done by the introduction of additional reagents and solvents, which might also result in the introduction of impurities into the reaction flask. In route 2, the reaction flask was opened as little as possible in order to minimize the possibility

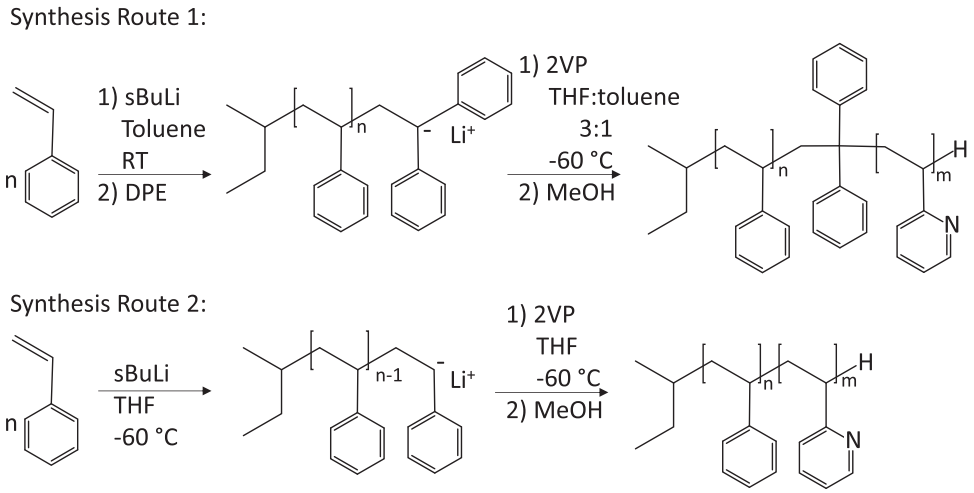

Figure 1. Two synthetic routes were used for the BCP samples in this study. Route 1: The PS block was synthesized in a nonpolar solvent for a slow polymerization and low $Đ$ of the PS block. The addition of DPE is supposed to suppress side reactions when adding 2VP. For solubility reasons, THF has to be added for the synthesis of the P2VP block. Route 2: The PS block and the P2VP block were both synthesized in the same solvent, and no DPE was added in order to conduct the reaction with as few steps as possible, to minimize possible sources of contamination by opening the reaction flask and introducing additional solvents or reactants.

of contamination. Both polymer blocks were synthesized in the same solvent, and no additional regents to control the reactivity were used.

Route 1: The PS block was synthesized in toluene at ambient temperatures inside an ampule. This was done to keep the dispersity $Đ$ of the polystyrene block as low as possible. In order to reduce the reactivity of the macroanion, 1,1-diphenylethylene (DPE) was added, and the reaction mixture was stirred for 2 h.

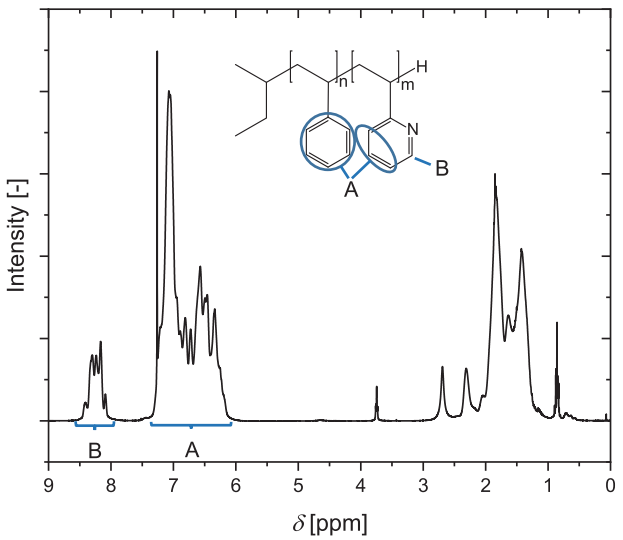

Figure 2. ^{1}H-NMR (400 MHz, $CDCl_3$) spectrum of PS-*b*-P2VP. Peaks related to the allylic backbone of the BCP have a chemical shift $\delta < 3$ ppm and the peak at $\delta = 3.74$ ppm belongs to leftover THF. The sample composition, or PS-fraction Φ_{PS} respectively, was calculated from the ratio of the peak integrals related to the aromatic protons of PS + P2VP (A) and only P2VP (B). This allows further to calculate M_n of the P2VP block and M_w via $Đ$ of the BCP.

Prior to the synthesis of the P2VP block, THF was distilled into a reaction flask or added from an ampule (9:1 THF/Toluene, e.g., 100 ml for 7 g PS-*b*-P2VP). The polar THF was added to prevent solubility issues when polymerizing the P2VP block. The solution of polystyrene macro anions in the solvent mixture was cooled to −50 °C. Subsequently, the 2VP was added under argon counter flow. The reaction mixture was stirred for 1 h at −50 °C and then stirred for 24 h at room temperature. The reaction was terminated by the addition of degassed methanol.

Route 2: The PS- and P2VP blocks were both synthesized in THF at −60 °C. The synthesis of the PS block was conducted under vigorous stirring for approximately 10 min, and after an aliquot was drawn for characterization, the 2VP monomer was added directly to the solution of PS-macro anions. The reaction was conducted for additional 10 min and then terminated by degassed methanol.

The product of both synthetic routes was precipitated in cold, low-boiling petroleum ether and dried at ca. 70 °C under reduced pressure.

2.3. Molecular Characterization

The PS-*b*-P2VP samples were labeled using the abbreviation of the polymer and the number average of the molecular weight in kg mol^{-1} in parenthesis. As an example, a polystyrene-b-poly-2-vinylpyridine with $M_n = 10$ kg mol^{-1} in each polymer block would be named PS(10.0)P2VP(10.0). The molecular weight of the polymer samples was determined via size exclusion chromatography (SEC). The SEC equipment was from Polymer Standard Service, (Mainz, Germany) specifically the Agilent 1200 series. Two PSS SDV Lux 300 × 8 mm i. d. columns with pore sizes of 10^3 and 10^5 Å were used. The solvent/mobile phase was THF stabilized with 250 ppm BHT at room temperature with a flow rate of 1 ml min^{-1}.

Table 1. Number average M_n, dispersity $Đ$ and volume fraction of the PS block Φ_{PS}. The PS block and $Đ$ of the BCP were obtained by SEC and $M_{n,\,P2VP}$ of the P2VP block was calculated from the intensities of characteristic peaks in ^{1}H NMR spectra. For the calculation of Φ_{PS}, a density ρ of 1.03 and 1.13 gcm^{-3} was used for PS and P2VP, respectively.[48] The PS-*b*-P2VP samples were labeled using the abbreviation of the polymer and the number average molecular weight in kg mol^{-1} in parenthesis. (a) This sample was synthesized using a different procedure (route 1) than the other samples (route 2).

sample abbreviation	$M_{n,\,PS}$ [g mol^{-1}]	$M_{n,\,P2VP}$ [g mol^{-1}]	$Đ$	Φ_{PS}
PS(7.2)P2VP(7.9)[b]	7 200	7 900	1.07	0.50
PS(8.4)P2VP(8.6)[a]	8 400	8 600	1.08	0.51
PS(8.9)P2VP(9.4)[b]	8 900	9 400	1.14	0.51
PS(23.4)P2VP(23.2)[b]	23 400	23 200	1.11	0.51

A Bruker Avance lll Microbay 400 MHz spectrometer was used to determine the molecular composition of the block copolymer samples in addition to the SEC-NMR measurements. The samples were dissolved in deuterated chloroform ($CDCl_3$, 99.8 %, Sigma–Aldrich) for the NMR experiments, and signals were referenced to the solvent peak at $\delta = 7.26$ ppm. Characteristic peaks at $\delta = 6.2$ to 7.3 ppm (aromatic; 5H for PS; 3H for P2VP; see **Figure 2**) in relation to the peak at $\delta = 8.3$ ppm (aromatic; 1H for P2VP) were used to calculate the molecular composition of the PS-*b*-P2VP BCP samples[48] (**Table 1**).

3. Morphological Characterization

3.1. Differential Scanning Calorimetry - DSC

To prove phase separation in the block copolymer, differential scanning calorimetry (DSC) measurements were conducted on a TA Q200 differential scanning calorimeter. The temperature ramp rate was 10 K min^{-1} and the heat flow curve of the second heating run was used for the determination of the glass transition temperatures T_g. The glass transition temperatures of the BCP samples are listed in **Table 2**. The PS and P2VP block, which are locally separated in domains consisting mainly of PS or P2VP, exhibit two separate glass transition temperatures from which the lower T_g was assigned to the P2VP block. The heat flow curves are displayed in **Figure 3**. The variability of the T_g values is partly caused by the molecular weight dependence of T_g. The DSC experiments were conducted with samples, that have been used in rheological experiments before, because they exhibit better separated steps of the heat flow curve than pristine samples. Thus, an improved separation of the polymer types by oscillatory shear is an additional influence parameter on the values of T_g.[52] This influence of the separation of polymer types by large amplitude oscillatory shear (LAOS) on T_g is exemplary displayed for one sample in the inset of Figure 3.

Table 2. Glass transition temperatures for the PS and P2VP block of the BCP samples. (a) This sample was synthesized using a different procedure (route 1) than the other samples (route 2), which may explain the comparably high T_{ODT}.

sample abbreviation	$T_{g,\,P2VP}$ [°C]	$T_{g,\,PS}$ [°C]	T_{ODT} [°C]
PS(7.2)P2VP(7.9)	82.8	96.2	162
PS(8.4)P2VP(8.6)[a]	79.2	94.8	228
PS(8.9)P2VP(9.4)	89.9	97.9	168
PS(23.4)P2VP(23.2)	86.7	100.7	–

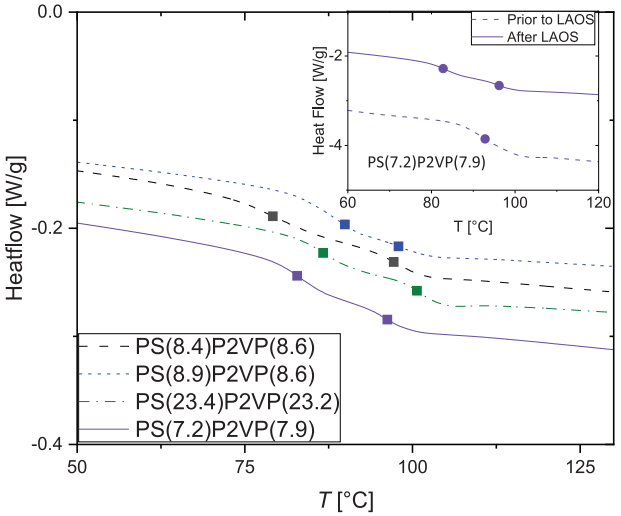

Figure 3. DSC graphs of the PS-*b*-P2VP samples used in this study. The second heating run with a temperature ramp rate of 10 K min^{-1} is displayed. Two separate glass transition temperatures T_g, which are marked by symbols, indicate separate PS and P2VP domains. The lower T_g is attributed to P2VP and the higher to PS. The variability of the T_g values is partly caused by the molecular weight dependence of T_g. A different degree of separation of the polymer types in the domains of their own type by oscillatory shear prior to DSC measurements, additionally increases the variability of T_g.[52] The inset displays this separation influence on the T_g of PS(7.2)P2VP(7.9). The parameters of the LAOS experiment were following: $\omega_1/2\pi = 1$ Hz, $\gamma_0 = 40$ %, $T = 160$ °C and $t = 1800$ s.

3.2. Small Angle X-Ray Scattering - SAXS

Small angle X-ray (SAXS) measurements were conducted on a Hecus S3-Micro X-ray system with a point microfocus source, 2D-X-ray mirrors, and a 2D CCD-detector from Photonic Science. A PW-H HKP300 press from P/O/Weber (Remshalden, Germany) was used for the sample preparation.

3.3. Rheology

Oscillatory shear measurements were performed on a strain-controlled ARES G2 rheometer (TA Instruments) equipped with a force rebalance transducer capable of measuring a torque range of 50 to 200 mNm. Experiments were either conducted using cone-plate or parallel-plate measurement tools with a diameter of 13 mm and a cone angle of 0.1 rad. Cone-plate combinations were used to ensure a homogeneous shear field in the sample, whereas the parallel plate setup was used if the rheological measurement itself (i.e., the correct measurement gap in experiments with a variation of temperature) or the subsequent sample analysis (i.e., well-defined spatial directions in SAXS measurements) benefited from it.

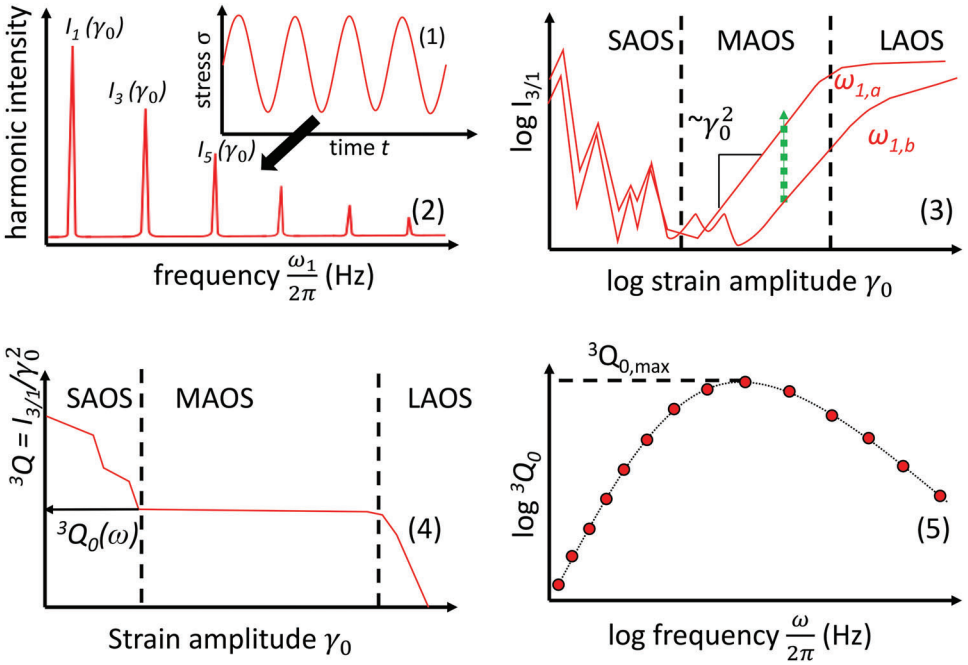

Figure 4. Scheme of a five-step procedure from raw data (1) to a nonlinear master curve (5). 1) Nonlinear stress time data of an oscillatory shear experiment. 2) After Fourier transformation of the time data, a magnitude frequency spectrum with odd higher harmonics can be obtained. 3) The ratio $I_{3/1}(\gamma_0, \omega_1)$ of the first and third harmonic is proportional to γ_0^2 in the MAOS region. For different frequencies $\omega_{1,a}$ and $\omega_{1,b}$ different developments of $I_{3/1}$ are observed, and data in between may be obtained by a dynamic frequency sweep experiment. 4) Extrapolation of $^3Q_0(\gamma_0, \omega_1)$ to small amplitudes gives the intrinsic nonlinearity $^3Q_0(\omega_1)$. 5) A nonlinear master curve can be created by plotting several $^3Q_0(\omega_1)$ values at different excitation frequencies, which are shifted to a reference temperature, utilizing the TTS principle. Reproduced with permission from Cziep, M. A.; Abbasi, M.; Heck, M.; Arens, L.; Wilhelm, M. *Macromolecules* **2016**, *49*, 3566–3579.[15] Copyright 2016, American Chemical Society.

3.4. Determination of T_{ODT}

When heating a homopolymer or a BCP melt of any kind, the dynamic storage modulus G' and the dynamic loss modulus G'' typically decrease steadily. However, in BCP melts, at the transition from the ordered state to the homogeneous melt, G' and G'' may decrease abruptly, indicating the sudden disappearance of phase boundaries at this first-order phase transition. To measure the T_{ODT} a temperature sweep experiment was performed over a large temperature range to find the temperature at which there was a sudden decrease in the dynamic moduli $G'(T)$ and $G''(T)$. Subsequent experiments over a narrower temperature range at low heating and cooling rates (1 K min^{-1}) were conducted to get more precise values for the transition temperature. All experiments were conducted under a nitrogen atmosphere to prevent oxidative degradation of the polymers. The heating and cooling procedure was repeated several times to ensure that the change in $G'(T)$ and $G''(T)$ originated from the order-disorder transition and not from thermal decomposition. A determination of T_{ODT} is also possible by other techniques such as DSC[48,53] or SAXS.[54–56] However, because of possible differences in calibration, and only little heat flow in DSC experiments at this transition, the rheological determination was used.

3.5. Experimental Determination of the Intrinsic Nonlinearity

The intrinsic nonlinearity can be determined by rheological experiments, in which the strain amplitude γ_0 is increased from the linear small amplitude oscillatory shear (SAOS) region to the medium (MAOS) and to the nonlinear large amplitude shear region (LAOS). This method using $I_{3/1}(\gamma_0)$ is described in detail in literature and also briefly in the following.[15,22] The determination of the intrinsic nonlinearity by strain sweep, as well as frequency sweep experiments is schematically displayed in **Figure 4**. The first two steps of the five-step procedure are done by the built-in rheometer software. Steps 3–5 display the procedure of the determination of a nonlinear master curve point by point from dynamic strain sweep (dss) experiments. If there is a common MAOS region for different frequencies at the same T ($\omega_{1,a}$ and $\omega_{1,b}$ in step 3), a dynamic frequency sweep (dfs) experiment with these frequencies and the ones in between enables the determination of the intrinsic nonlinearity after division of $I_{3/1}$ by γ_0^2. The advantages of this technique are a reduction in sample loadings, the obtaining of more data per experiment, and a more direct measurement of the development of the nonlinearity in dependence of a frequency or frequency-related unit.

This measurement method requires multiple sample loadings related to sample failure, such as edge fracture, or a change in the sample caused by the large deformation, which is especially relevant for block copolymers, in which domains are aligned by the oscillatory shear in the mechanical nonlinear regime.[57] Thus, the dynamic strain sweep experiments at different temperatures were used as probing experiments for the MAOS region at these temperatures. The number of sample loadings can be reduced by a determination of the intrinsic nonlinearity by experiments in the previously determined MAOS regime with only a variation of the oscillation frequency $\omega_1/2\pi$. This procedure to obtain

$I_{3/1}(\omega)$ is described in detail in the literature and is schematically displayed in Figure 4.[58] To minimize the influence of sample loadings and a possible orientation of domains on the intrinsic nonlinearity and to obtain additional information, an approach similar to the one with a varying $\omega_1/2\pi$ was used: The MAOS region for different temperatures was determined by probing strain sweep experiments at these temperatures. For the final determination of the intrinsic nonlinearity, $\omega_1/2\pi$ and γ_0, which are in the MAOS regime of the probing experiments at multiple temperatures, were chosen. The melt was then sheared using these rheological parameters, $\omega_1/2\pi$ and γ_0, while varying T gradually in a temperature sweep experiment to obtain $I_{3/1}(T)$. For some samples, the same parameters could be used to create the nonlinear master curve for the whole temperature range. For other samples, such as PS(23.4)P2VP(23.2), γ_0 had to be changed in between different temperature regions in order to keep the same level of nonlinear response. The influence of γ_0 on the measured value of $I_{3/1}$ was eliminated by a division by γ_0^2, as it is also done at the determination of the intrinsic nonlinearity by frequency sweep experiments. This measurement procedure, with only a variation of temperature, is supposed to reduce the influence of sample loadings, previous measurements and different degrees of domain alignment related to this. Compared to the determination of the intrinsic nonlinearity by a variation of γ_0 or $\omega_1/2\pi$, which shows only a snapshot of the intrinsic nonlinearity for certain temperatures (i.e., $\Delta T = 10{\sim}K$), the gradual variation of T directly shows the respective nonlinear behavior of the material. For samples with an accessible T_{ODT} this approach can give additional information, such as the influence of phase boundaries on the intrinsic nonlinearity of the polymer melt.

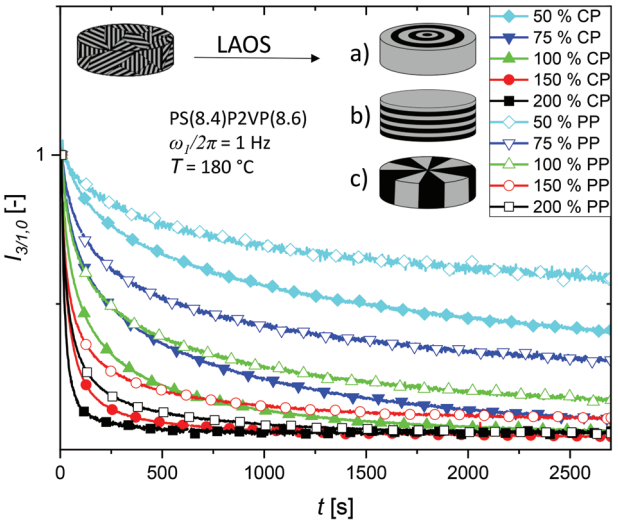

Figure 5. Influence of γ_0 and the measurement geometry on the domain alignment monitored by the evolution of $I_{3/1}$ normalized to its value at t = 0 s. Domain alignment by previous experiments and sample loading was erased by heating the sample above its T_{ODT}. The domains align faster at higher strain amplitudes γ_0. This is reflected by a faster alignment in a cone-plate geometry (CP, homogeneous shear field) compared to an alignment experiment with identical parameters with a parallel-plate geometry (PP, shear field gradient from $\gamma_{local} = \gamma_0$ at the sample rim, towards γ_{local} = 0 % in the center of the sample). For a similar volume fraction Φ of the unlike polymer blocks, diblock copolymers exhibit a lamellar morphology. Possible lamellar orientations such as the a) perpendicular, b) parallel and c) transverse are shown, but only the perpendicular one (a) and the parallel (b) were observed for the displayed experiments.

4. Results and Discussion

The alignment of domains using large amplitude oscillatory shear can be monitored by the time evolution of the mechanical moduli or higher harmonics such as $I_{3/1}$. This evolution is already an indication, that experiments with phase separating systems contain a time (t) dependent component, which poses additional challenges for measurements of these systems. As an example, the time evolution of $I_{3/1}(t)$ of the sample PS(8.4)P2VP(8.6) with varying stain amplitudes γ_0 and measurement tools (cone-plate & parallel-plate) is displayed in **Figure 5**. Possible domain alignment caused by previous experiments or sample loading was erased by heating the sample above its T_{ODT} between the alignment experiments, and $I_{3/1}$ is normalized to its value at the beginning of the experiments. For the displayed experiments of this sample only the perpendicular orientation, see Figure 5, was determined by ex-situ SAXS experiments.

The sample PS(8.4)P2VP(8.6) exhibits an unusually high T_{ODT} at 228 °C, compared to the other PS-*b*-P2VP samples used in this study. This may be explained by the different synthetic procedure of this sample, in which DPE was used to reduce the reactivity of the PS macro anion and to prevent side reactions at the pyridine ring.[59–61] Minor differences in $Đ$ or a slight difference in molecular weight, i.e., by not taking the aromatic protons of DPE into consideration, cannot explain this deviation from the expected dependence of the phase transition on temperature. In contrast, the addition of DPE, which is still present in the final BCP directly at the connection of PS and P2VP, may explain the high T_{ODT}. On the one side, the total degree of polymerization N is a quantity that defines the strength of phase separation and is only changed by $\Delta N = 1$, considering the DPE equivalent to a single monomer unit. On the other hand, DPE is known to be able to stiffen a polymer chain by the two bulky aromatic rings and thus has, in larger fractions in a polymer chain, even an influence on chain end related properties such as the T_g of the polymer.[62] The stiffening of the polymer chain directly at the connection of the PS and P2VP separates the polymer sorts directly at their interface, which may shift the *ODT* toward a higher temperature.

Changes in the material properties are most pronounced close to the beginning of the experiment, which can be explained by a comparably fast alignment of lamellae from an unfavorable orientation in the shear field to a favorable orientation and a slower defect annihilation afterward.[32] Thus, treatment of a sample with completely non-aligned domains in the melt (i.e., adjustments of the gap between the geometry surfaces) is supposed to have a comparably larger influence than the treatment of an already partially aligned sample. The higher γ_0, the faster the alignment of the domains, which also holds for the comparison of a cone-plate geometry with a homogeneous shear field and a plate-plate geometry, in which there is a gradient of $\gamma_{0,max}$ toward $\gamma_0 = 0$ in the center of the sample. Thus, the domain alignment accelerates during a dynamic strain sweep experiment, which could be used to determine the intrinsic nonlinearity of homopolymers. The dependence on γ_0 additionally illustrates why the intrinsic nonlinearity of BCP melts cannot simply be determined with an inhomogeneous

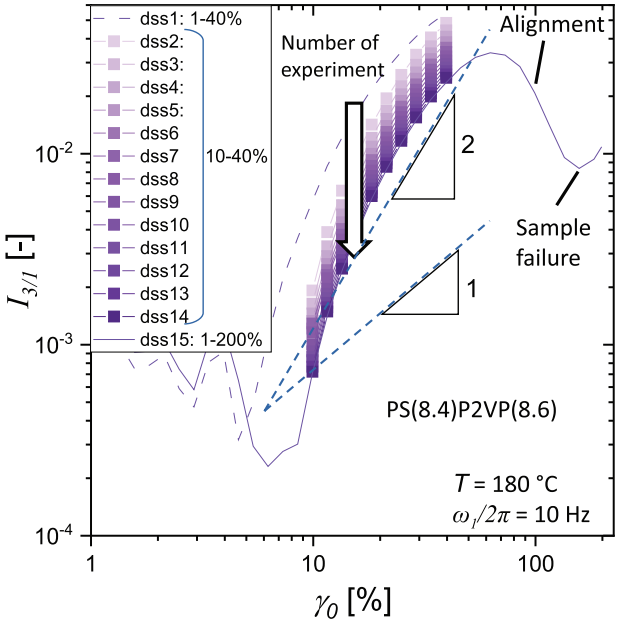

Figure 6. Consecutive dynamic strain sweep (dss) experiments of PS(8.4)P2VP(8.6) with unaligned domains ($\omega_1/2\pi$ = 10 Hz, γ_0 = 1 - 40 %, γ_0 = 10 - 40 % and γ_0 = 1 - 200 % in the last dss experiment, respectively). The domains are aligned during the dss experiments, resulting in a decrease of $I_{3/1}$. The γ_0-dependence of $I_{3/1}$ is overshadowed by the domain alignment, which illustrates the necessity to do dss experiments on well-aligned samples. For $\gamma_0 \geq 40\%$ the domain alignment is amplified, resulting in a drastic decrease of $I_{3/1}$. The increase of $I_{3/1}$ at the end of the experiments indicates sample failure, such as edge fracture or outflow. Dashed lines indicate slopes of 1 and 2. A slope of 2 is common for homopolymer melts. The slope of the BCP melt exceeds this slope, but is gradually decreasing with an increasing number of dss experiments or shearing in the nonlinear mechanical regime, respectively. For prolonged shear under LAOS conditions, the slope further decreases toward a slope of 1, see Figure 8.

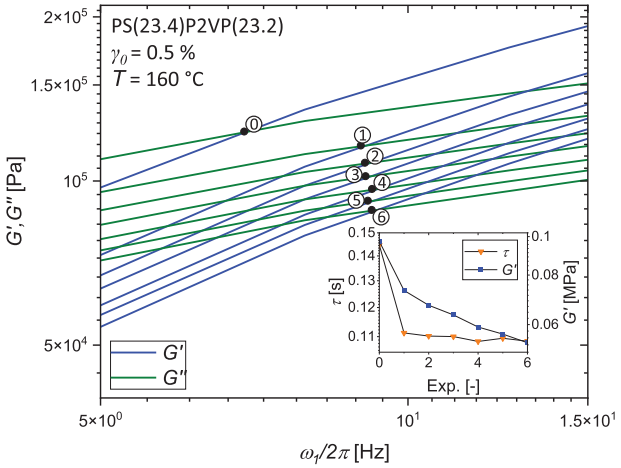

Figure 7. Frequency-dependent mechanical moduli G' and G'' of PS(23.4)P2VP(23.2) in dependence of the number of alignment experiments. The measurement (0) was conducted before aligning the lamellae. The influence of lamellae alignment on the terminal relaxation time τ, which is obtained by the crossover of G' and G'', illustrates challenges for determining a frequency-dependent intrinsic nonlinearity $^3Q_0(\omega)$ of a phase separated BCP melt. The mechanical moduli decrease in a series of alternating alignment and frequency sweep experiments and their crossover shifts to higher angular frequencies, reflecting a decrease of τ. The inset displays τ in dependence of the alignment experiment with $\omega_1/2\pi$ = 0.5 Hz, γ_0 = 100 %, T = 160 °C for a duration of t = 60 s, as well as G' at $\omega_1/2\pi$ = 50 Hz after the individual alignment experiments. The development of τ and G' resembles the development in a typical domain alignment experiment, as shown in Figure 5. The lamellae were aligned in the parallel orientation, as determined by ex situ SAXS experiments.

shear field and calculated for a homogeneous shear field as possible for other polymer systems.[63,64] The influence of the domain alignment on $I_{3/1}(t)$ is best determined in the alignment experiment with γ_0 = 150 and 200 % in a homogeneous shear field (CP), because only in these experiments a clear plateau of $I_3/1$ is achieved in the alignment experiment.

A series of experiments with increasing γ_0 for the sample PS(8.4)P2VP(8.6), which shows the typical development of $I_{3/1}$ observed for phase separated BCP melts, is displayed in **Figure 6**. A domain alignment was erased beforehand by heating the sample above its T_{ODT}. The value of $I_{3/1}$ does not show the expected dependency on γ_0 of γ_0^2, which is observed for other polymers, but a higher exponent, which is attributed to the polymer interface.[15,64,65] The experiments were stopped before the occurrence of sample failure, such as edge fracture or outflow, and a decrease of $I_{3/1}$ for consecutive measurements was observed. The occurrence of problems at the edge of the sample may be reduced by the use of partitioned geometries in further studies.[15,46] In this study, sample failure was monitored in situ by the appearance of even higher harmonics such as $I_{2/1}$, that are normally symmetry-forbidden.[66,67] The decrease of $I_{3/1}$ relative to previous measurements is most pronounced for the early experiments of the series, which is in agreement with alignment experiments (see Figure 5). For a higher γ_0 the absolute nonlinearity decreases with the increasing alignment of lamellae. The slope of $I_{3/1}$ between γ_0 = 10 and 40 % changes most between the first and second strain sweep experiment, which is in agreement with the largest changes in the material properties at the beginning of an alignment experiment. An increase of $I_{3/1}$ at $\gamma_0 \geq 100$ % is caused by sample failure, which was indicated by the occurrence of even higher harmonics such as $I_{2/1}$ The values of $I_{3/1}$ at low strain amplitudes, e.g., in Figures 6, 8 and 10, result from a constant noise originating from the rheometer. When I_3 is noise and $I_1 \propto \gamma^1$, then $I_{3/1}$ has to decrease with $I_{3/1} \propto \gamma^{-1}$ at low strain amplitudes, as a consequence.[68]

The influence of domain alignment on $I_{3/1}$ is reflected by the terminal relaxation time τ of the BCP, which is also referred to 'longest relaxation time'. However, due to an additional structural relaxation in BCP melts, which is orders of magnitude larger, the term 'terminal relaxation' is more appropriate.[69] For the entangled sample PS(23.4)P2VP(23.2) the influence of domain alignment on τ is displayed in **Figure 7**. The lamellae were increasingly aligned parallel, as determined by SAXS. Block copolymer chains can more easily move in directions along the interface between the polymer blocks than orthogonal to the interface.[70] Thus, aligning the lamellae reduces the amount of boundaries between differently oriented polymer grains, which otherwise constrain the polymer chains in their movement and increase the terminal relaxation time. Thus, with an increasing degree of alignment of the domains, τ decreases, and thus $I_{3/1}$.

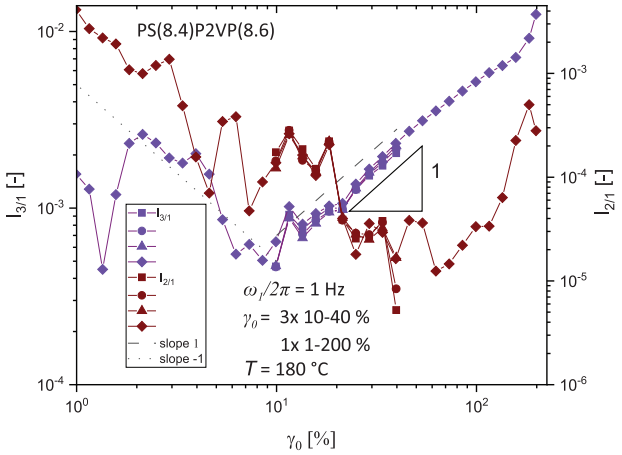

Figure 8. Strain sweep experiment with perpendicularly aligned domains of PS(8.4)P2VP(8.6). The dashed line indicates a slope of $I_{3/1} \propto \gamma_0^{\alpha}$; $\alpha = 1$. Prior to domain alignment by LAOS (see Figure S7, Supporting Information for the alignment experiment), the slope was close to 2, see Figure 7. The reduced slope is attributed to changes in the polymer chain relaxation due to domain alignment. Even higher harmonics only appear if the measured stress s not equal in both oscillation directions and can be used to show problems with the sample, such as edge fracture.[66] The presence of $I_{2/1}$ at a low γ_0 results from a constant noise of I_2, which is divided by $I_1 (\propto \gamma_0^1)$ and thus scales with γ_0^{-1} for γ_0, at which I_2 is below the level of noise. The value at $\gamma_0 \approx 100$ % indicates sample problems, which is reflected by a sudden increase of $I_{3/1}$ at this strain amplitude γ_0.

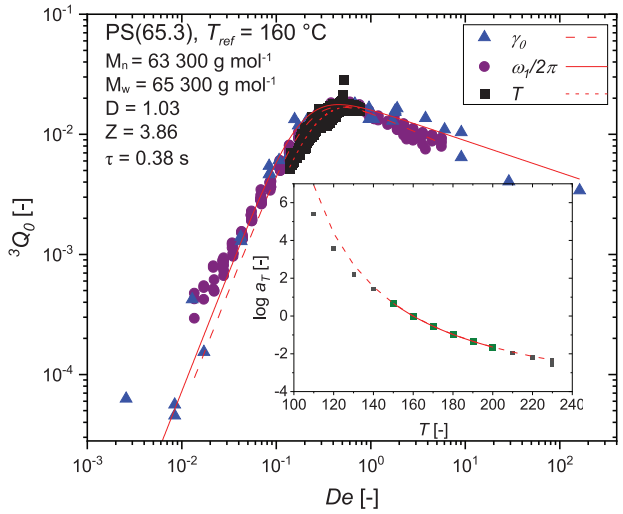

Figure 9. Comparison of $^3Q_0$ of a polystyrene homopolymer determined by different measurement techniques, in which γ_0, $\omega_1/2\pi$, or T is varied, and the respective data fit by Equation (1) (red lines). The determination of the intrinsic nonlinearity by a variation of temperature was used on a well-investigated, simple polymer system (entangled linear homopolymer melt) to evaluate the suitability for creating nonlinear master curves and the possible use for investigations of the intrinsic nonlinearity of BCP melts. The inset shows the a_T shift factors. The fit by the WLF equation to the highlighted factors was used for the interpolation of shift factors in the determination of $^3Q_0$ by a variation of temperature.

The dependence of the nonlinearity on the degree of alignment of domains may be erased by measurements of samples with completely aligned domains, which are indicated by constant material properties, see Figure 5. Experiments at temperatures above T_{ODT} not only erase the influence of alignment, but also prevent the determination of the influence of phase boundaries on the relaxation process of the BCP chains.

A series of strain sweep experiments of the sample PS(8.4)P2VP(8.6) with aligned lamellae is displayed in **Figure 8** and the rheological data of the respective alignment experiment can be found in the Supporting Information (Figure S10, Supporting Information). The experiment was repeated with and without waiting between the individual dynamic strain sweep experiments to evaluate a possible influence on the dependency of $I_{3/1}$ on γ_0, but resulted in the same slope within the limit of the experimental error of one experimental series. The even higher harmonic $I_{2/1}$ was monitored during the alignment experiment to detect sample failure, which would be indicated by an increase of its value. The strain dependency of $I_{3/1}$ of the perpendicular aligned PS(8.4)P2VP(8.6) is displayed in Figure 8. The proportionality of $I_{3/1}$ on γ_0^{α} was determined to be close to $\alpha = 1$, as indicated by the dashed line with a slope of 1.

4.1. Determination of the Intrinsic Nonlinearity by a Variation of Temperature

Before determining the intrinsic nonlinearity in BCP melts by a variation of temperature, this technique was first tested on a simpler polymer system, a linear polystyrene homopolymer sample. The molecular characteristics of the PS sample are listed in the top of **Figure 9**. The intrinsic nonlinearity of the PS sample determined by the three measurement methods is displayed in the same figure and shows, that the approaches describe a similar development of $^3Q_0$. The data was fitted by the following empiric equation, whose derivation is described in detail in literature:[15]

$$^3Q_0(De, Z) = 0.32 Z^{-0.5} \frac{De}{1 + 33.8 Z^{-1} De^{2+0.35}} \quad (1)$$

The intrinsic nonlinearity of homopolymers $^3Q_0$ at a specific frequency or Deborah number De, respectively, is only a function of the number of entanglements Z. The values of $^3Q_0(De, Z)$ determined by strain sweep experiments and fitted by Equation (1) were used as a reference. The maximum of $^3Q_0$ was 1.69×10^{-2} and 1.67×10^{-2} or 4.5 % lower and 4.4 % lower, compared to the reference (1.77×10^{-2}) if $^3Q_0$ was determined by a variation of T or $\omega_1/2\pi$. For shifting the nonlinear data, which was obtained by the temperature sweep approach at one specific ω_1, to another ω_1 or De respectively, the a_T-shift factors in this temperature range have to be interpolated. This data fit by the Williams-Landel-Ferry equation (WLF), which describes the temperature dependence of relaxation mechanisms in amorphous polymers, and the interpolation of the a_T-shift factors is displayed in the inset of Figure 9.[71]

4.2. Intrinsic Nonlinearity of Block Copolymer Melts

For a general description of the nonlinear polymer melt behavior, the frequency-dependent intrinsic nonlinearity $^3Q_0(\omega, Z)$ can be plotted against the Deborah number De, as displayed in Figure 9 for a PS homopolymer melt. A similar plot could be done for BCP melts since temperature and $\omega_1/2\pi$ are known and a_T-shift

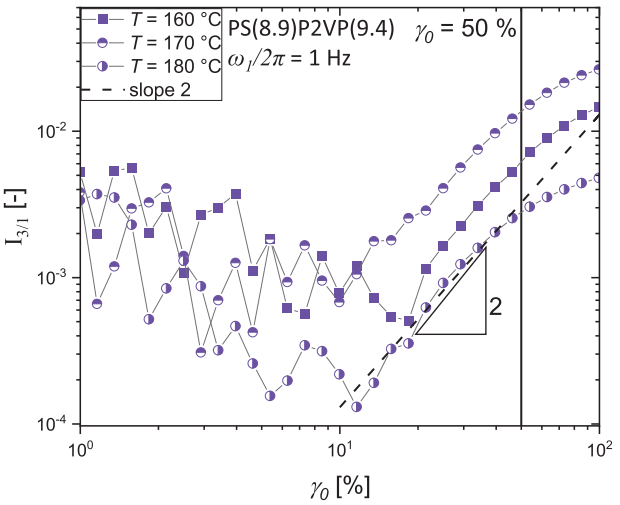

Figure 10. Dynamic strain experiments on PS(8.9)P2VP(9.4) above and below T_{ODT} (T_{ODT} = 168 °C, see Table 2) show a dependency of $I_{3/1}$ close to γ_0^2. The vertical line indicates the strain amplitude of $\gamma_0 = 50$ % at which the intrinsic nonlinearity was determined, as shown in Figure 11.

factors can be interpolated by the WLF-equation as for the PS melt in Figure 9. However, this generalization was avoided for BCP melts, because it would result in misleading graphs with frequency-dependent phase transitions.

To determine the influence of phase boundaries on the nonlinearity without the influence of domain orientation PS(8.9)P2VP(9.4) was cooled from above T_{ODT} (T_{ODT} = 168 °C) to below while shearing the melt in the MAOS regime ($\gamma_0 = 50$ %). The rheological parameters for the temperature sweep experiment were determined by strain sweep experiments in the temperature range under investigation before (see **Figure 10**). The scaling of $I_{3/1}$ on γ_0^{α} was (close to)$\alpha = 2$, which is expected for homopolymer melts. To eliminate the dependency of $I_{3/1}$ on γ_0 and evaluate the measured data as the one of homopolymer polymer melts by ${}^3Q_0$, $I_{3/1}$ was divided by γ_0^2.

The nonlinearity of PS(8.9)P2VP(9.4) describes the development shown in **Figure 11** with a maximum close to, but slightly above, the T_{ODT} of this sample, an order of magnitude decrease of $I_{3/1}$ around T_{ODT} and a subsequent domain alignment experiment at $T < T_{ODT}$. The domain alignment shows the typical development with the largest change of $I_{3/1}$, G' and G'' shortly after the start of the alignment. While the lamellae align in the shear field, these observables normally decrease until a plateau value is reached, as displayed for PS(8.4)P2VP(8.6) in Figure 5. In the experiment, which is displayed in Figure 11, no plateau of the observables can be reached due to the constant decrease of the temperature and the associated increase of the mechanical moduli, as well as $I_{3/1}$. After the domains are mostly aligned, $I_{3/1}$ increases linearly with decreasing temperature. The obtained lamellar orientation was determined to be perpendicular by SAXS. The nonlinearity in the intermediate region, between the homogeneous melt and the melt with aligned lamellae, has to be considered with caution as the development of $I_{3/1}$ depends on γ_0. The influence of γ_0 cannot be eliminated by a simple division, because the time needed for the domains to align, and thus the slope of $I_{3/1}$ vs. $1/T$, is inversely proportional to γ_0. The origin of the nonlinearity in the BCP melt and not in other effects, such as edge fracture, was confirmed by conducting the experiment multiple times, as shown in the Supporting Information. The repetition of the experiment additionally confirmed the applicability of determining the nonlinearity by a variation of temperature. The maximum of ${}^3Q_0$ above T_{ODT} was confirmed by heating and cooling the melt multiple times without a shift on the T-axis.

To check if the maximum of ${}^3Q_0$ close to T_{ODT} is a general feature of BCP melts or unique to the investigated sample, the nonlinearity of PS(7.2)P2VP(7.9) was determined for temperatures around its T_{ODT} (= 162 °C), which is displayed in **Figure 12**. Additionally, the influence of domain alignment was evaluated by heating the sample with aligned domains above its T_{ODT} while monitoring its nonlinearity and conducting temperature sweep experiments with increasing and decreasing temperature, respectively. A parallel lamellar orientation was determined by SAXS. When heating the sample, a behavior similar to a strong strain overshoot, with an increase in both G' and G'', is observed.[72,73] Unlike for a strain overshoot, in the case of the BCP melt around T_{ODT}, the strain is kept constant. However, the alignment of domains facilitates chain relaxation (see the reduction of τ_0 as a function of experiments in Figure 7) and as soon as the interface between the polymer domains disappears, τ_0 as well as the stress σ in the system shortly increases, which results in the observed behavior.

When cooling PS(7.2)P2VP(7.9) only an increase of ${}^3Q_0$ above the previously determined T_{ODT} could be observed, as it is shown in Figure 12, and a clear maximum only appears when cooling below T_{ODT}. The development of ${}^3Q_0$ toward lower temperatures appears to approach a maximum, similar as for PS(8.9)P2VP(9.4) in Figure 11. However, the maximum for PS(7.2)P2VP(7.9) would be extrapolated to be at T = 162 °C and thus at or even slightly below (1 K) the T_{ODT} of this sample. Taking the data below T_{ODT} into account, a maximum of ${}^3Q_0$ could be determined. However, the position of this maximum is influenced by the alignment below T_{ODT} and thus is determined to be at 164 °C, a temperature at

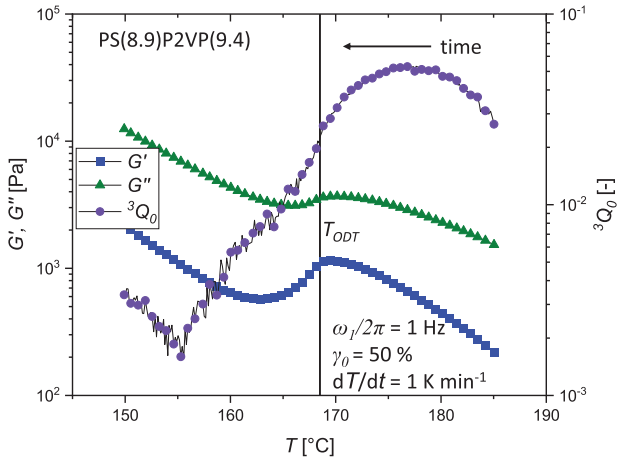

Figure 11. When cooling PS(8.9)P2VP(9.4) from above to below T_{ODT} while shearing with $\omega_1/2\pi = 1$ Hz, $\gamma_0 = 50$ %, a maximum of ${}^3Q_0$ is passed about $\Delta T = 10$ K before the melt phase separates and the formed lamellae are aligned in the shear field. The lamellar orientation was perpendicular, as determined by ex situ SAXS experiments.

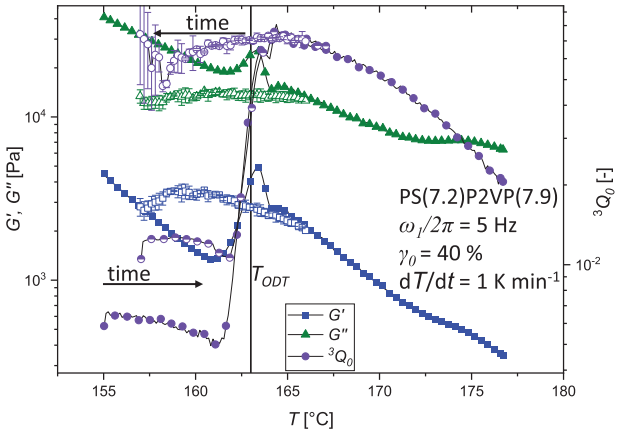

Figure 12. Summary of multiple experiments with heating and cooling the melt of PS(7.2)P2VP(7.9) over its phase transition. The BCP melt displays a hysteresis regarding G', G'' and $^3Q_0$ as well. When cooling past T_{ODT}, (empty circles) domains are aligned and the observables decrease following this alignment process. When heating, (filled and half filled circles) the observables show a sudden increase at the transition to the homogeneous melt. The nonlinearity of the melt in the separated state depends on the degree of domain alignment, and thus, a better aligned sample (filled circles) displays a lower $^3Q_0$ than a less aligned sample (half filled circles). The lamellar orientation was determined to be parallel by ex situ SAXS experiments, see Figure 5b.

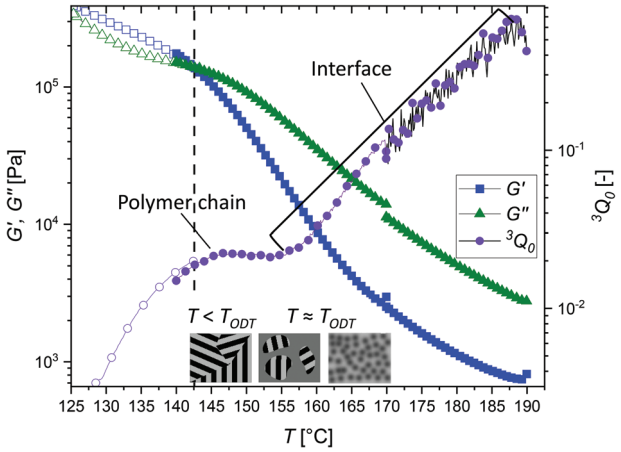

Figure 13. Mechanical moduli G' and G'' and $^3Q_0$ in dependency of T. Empty symbols display data shifted using the TTS principle. The overall nonlinearity of PS(23.4)P2VP(23.2) is dominated by the one originating at the interface or polymer block connection point, respectively. For this sample with an entangled PS block a second maximum around 143 °C is found, which is associated with the nonlinear contribution from the polymer chain. The maximum from the interface is around two decades higher than the one originating from the polymer chain, and the temperature dependence of $^3Q_0$ overshadows the one for a homopolymer chain. In the bottom, possible interfaces are displayed, which are present only in the phase separated state (left) or at the onset of phase separation (right).

which the maximum was not found when cooling the melt. The kinetics of domain alignment in Figure 12 are slower compared to Figure 11 due to a lower γ_0 ($\gamma_0 = 40$ % instead of $\gamma_0 = 50$ %) and additionally a lower T ($T < 162$ °C instead of $T < 168$ °C) The influence of the domain alignment on the nonlinearity can be seen by comparing the values of $^3Q_0$ below T_{ODT} in Figure 12. The domains were aligned using the same rheological parameters ($\gamma_0 =$ 50 %, $\omega_1/2\pi = 5$ Hz; see Figure S9 (Supporting Information) for the data relating to the domain alignment), but due to different temperatures ($T_1 = 155$ °C, $T_2 = 157$ °C) were aligned to a different extent. At a higher temperature, the domains are aligned to a greater extent in the same time frame due to a higher mobility in the polymer melt, which is reflected in a lower $I_{3/1}$.

The temperature at which the maximum of $^3Q_0$ is found is influenced by relaxation processes, which are also reflected in the linear data. The sample PS(8.9)P2VP(9.4) exhibits nearly a modulus crossover in the linear data (see Figure S4, Supporting Information), which correlates with a maximum in $^3Q_0$ for homopolymers of different topologies.[15,18,22] A shift of the frequency at the minimum of tan δ (tan $\delta = G''/G'$) using the time-temperature superposition principle, would result in a maximum of $^3Q_0$ at a temperature above 178 °C. Thus, the shift of $^3Q_0$ to a temperature above T_{ODT}, probably results from including these additional contributions to $^3Q_0$. For the other PS-*b*-P2VP samples, the moduli of the linear data do not approach each other as close as for PS(8.9)P2VP(9.4). Thus, the maximum in $^3Q_0$ is less affected by these contributions for the other samples than PS(8.9)P2VP(9.4).

The nonlinear behavior of a BCP with an inaccessible T_{ODT} was determined to get insight on a possible relation between the maximum in nonlinearity and the phase transition. The BCP PS(23.4)P2VP(23.2) showed the nonlinear behavior in **Figure 13**, in which $^3Q_0$ increased towards higher temperatures, similar to the previously shown examples. However, no T_{ODT} could be determined even for heating above the shown temperature window (measurements up to $T = 260$ °C). The domains of the sample were partly aligned parallel, as determined by SAXS, prior to the determination of the nonlinearity. The domains were aligned in order to decrease the influence of sample handling on the development of $I_{3/1}$. The development of the nonlinearity showed a kink toward higher values of $I_{3/1}(T)$ at low temperatures. Data of $I_{3/1}(T)$, which was measured at the same temperature range, but with higher $\omega_1/2\pi$ and then shifted to lower temperatures, unveiled a second maximum, which can be attributed to the polymer chain itself. For shifting the data, the time-temperature superposition principle (TTS) was used, but data was shifted to a different temperature instead of a different frequency. The sample PS(23.4)P2VP(23.2) is the only sample in this study with a molecular weight of the polymer blocks above the entanglement molecular weight of the respective polymer type. Thus, the stress relaxation of this sample can be determined by a crossover of G' and G'' in the linear viscoelastic region, which correlates to the maximum of the intrinsic nonlinearity.[15] When aligning the domains of the BCP melt, the maximum of $I_{3/1}$, or $^3Q_0$ respectively, shifts to lower $\omega_1/2\pi$ along with the modulus crossover in the terminal regime of the polymer melt, as shown in **Figure 14**. This crossover is related to the structural relaxation.[74] This shift of the structural relaxation is opposite to the shift of the modulus crossover at the lower frequency of the rubber plateau between the individual alignment experiments, which describes the single chain dynamics (shift to higher $\omega_1/2\pi$; see Figure 7). The shift to lower frequencies is more expressed for the modulus crossover than for the maximum of $I_{3/1}$ as observed for other BCP systems before[74]. The data shown in Figure 14 results from three consecutive measurements, and the error bars of the mechanical

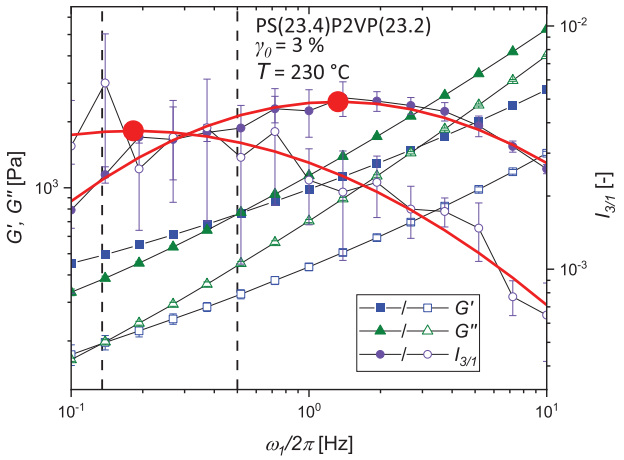

Figure 14. Frequency dependent mechanical moduli G' and G'' and $I_{3/1}$ before (filled symbols) and after (empty symbols) domain alignment. The red line indicates a fit to the data of $I_{3/1}$ with a dot at its maximum. The maximum in $I_{3/1}$ shifts to lower frequencies if the lamellae are (further) aligned. The shift of the maximum of $I_{3/1}$ is correlated to a shift of the modulus crossover in the flow zone of the sample, which is associated with an interaction with the phase boundary. The maxima of $I_{3/1}$ are determined via a fit by a Gauss function to the logarithmic values of $I_{3/1}$ and $\omega_1/2\pi$.

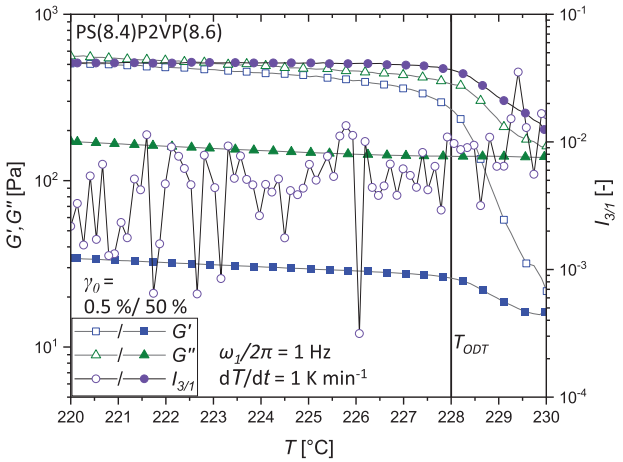

Figure 15. The influence of the interface on G' and G'' is more expressed in the SAOS regime, in which G' and G'' both change drastically at the phase transition, than in the MAOS regime, in which only an influence on G' is noticeable. The T_{ODT} is indicated as a vertical line. Data, which was measured with $\gamma_0 = 0.5$ % is displayed as empty symbols and with $\gamma_0 = 50$ % as filled symbols. The lamellae of this sample were aligned perpendicular, as determined by ex-situ SAXS experiments.

moduli are hardly visible, whereas $^3Q_0$ shows strong scattering, especially in the low frequency range. Increasing γ_0 leads to additional domain alignment and changes of G' and G'' within the measurement series, and thus there is no option for determining an experimental error of G', G'' and $I_{3/1}(\omega_1)$.

Different interfaces are displayed at the bottom of Figure 13, which could relate to nonlinearity at different temperatures. These are, from left to right, the interface between differently oriented polymer grains, or an interface between phase separated and homogeneous regions in the polymer melt, and a gradually with temperature changing interface between the two unlike polymers. However, some interfaces, such as the interface between differently oriented polymer grains (left), can only be found at $T < T_{ODT}$ and thus do not explain nonlinearity or even a maximum above T_{ODT} like displayed in Figure 11. The formation of phase separated regions in the homogeneous polymer melt at temperatures around T_{ODT} (middle) cannot explain an increase in nonlinearity toward T_{ODT} from temperatures below. Additionally, this interface is only reasonable for different temperatures within the sample and, thus, phase separated and non-separated regions in the BCP melt. The only interface, which is present at all temperatures and is different from the case of homopolymer melts, is a gradually changing interface at $T \sim T_{ODT}$. When cooling the BCP melt, the Flory-Huggins parameter χ and thus the strength of phase separation increase, which causes nonlinearity if a polymer is forced through a region of predominantly the opposite polymer. In a well-aligned BCP melt, the unlike polymers are spatially separated in their own lamellae. For less aligned samples, the distribution profile is less sharp, and polymer blocks in the opposite polymer are contributing to $^3Q_0$, which can be concluded from the different degrees of alignment in Figure 12. When approaching T_{ODT} with an only marginally sheared melt, as displayed in Figure 13, the polymer blocks in the unlike lamellae exhibit a with temperature gradually increasing $^3Q_0(T)$.

The appearance of $^3Q_0$ in proximity to the modulus crossover in the flow zone of the BCP melt and mutual shift by domain alignment additionally suggests a correlation of $^3Q_0$ to the degree of aligned domains and thus the fraction of polymer chains in the lamella of the opposite polymer type. The value of $^3Q_0$ at a similar temperature was investigated for PS(8.4)P2VP(8.6), with its T_{ODT} close to the temperature at the nonlinearity maximum of PS(23.4)P2VP(23.2). The value of $^3Q_0$ for PS(8.4)P2VP(8.6) increased toward 0.16, see **Figure 15** for the raw data, a similar value as for the other non-entangled samples, when transitioning from the homogeneous to the phase separated melt. This is one indication that the value of $^3Q_0$ is related to N, which is observed for homopolymer melts to only a minor extent.[15] The development of nonlinearity toward the phase separated state is opposite to that for the other non-entangled samples, see Figure 11 or Figure 12, in which $^3Q_0$ is found to be higher at T_{ODT} or above and thus in the homogeneous melt. This suggests a contribution of the polymer chain itself, as the nonlinearity originating from a homopolymer chain decreases with increasing temperature, and the influence on the overall nonlinearity can be seen for PS(23.4)P2VP(23.2) in Figure 13. The temperature at which T_{ODT} is found appears to have no remarkable influence on the value of $^3Q_0$. It differs for the non-entangled samples with a similar N but a difference in T_{ODT} of 63 K only to a minor extent. The highest value of $^3Q_0$ for PS(8.9)P2VP(9.4), PS(7.2)P2VP(7.9) and PS(8.4)P2VP(8.6) are determined to be $^3Q_0 \approx 5 \times 10^{-2}$, 7×10^{-2} and 16×10^{-2}, respectively. The increase of N and thus the strength of phase separation, however, results in a drastic increase of $^3Q_0$ as it can be seen in a comparison of the PS-*b*-P2VP samples with non-entangled polymer blocks and PS(23.4)P2VP(23.4), for which a $^3Q_0 \approx 6 \times 10^{-1}$ is obtained, see Figure 13. This additionally supports the movement of polymer chains through the lamellae of the opposite polymer type as a major contribution to $^3Q_0$.

5. Conclusion

In this study, the influence of phase boundaries in lamellae forming PS-*b*-P2VP BCPs on the nonlinearity of the polymer melt, specifically $I_{3/1}(T)$, was investigated. The domain alignment during the determination of the nonlinear melt behavior complicates this determination in a continuously changing system, and thus a different measurement approach had to be developed. The interplay between relaxation processes and the excitation frequency was varied by a gradual variation of the temperature. By this approach, the influence of the phase boundary on the intrinsic nonlinearity ${}^3Q_0$ could be measured, and the melt behavior directly at the transition from a homogeneous melt to a phase separated system, which would be hidden for other measurement techniques, could be unveiled. The major contribution to ${}^3Q_0$ was attributed to polymer chains in the lamellae of the opposite polymer type with an increase toward T_{ODT}, where the unlike polymer sorts are mixed the most in the phase separated melt or exhibit the highest separation strength in the not separated melt, respectively. The nonlinearity originating in the phase boundary or polymer chains in the lamellae of the opposite polymer type was found to be significantly higher than the nonlinearity attributed to polymer chain relaxation (≈2 orders of magnitude in ${}^3Q_0$). The maximum of ${}^3Q_0$ correlates with the crossover of G' and G'' in the flow zone of the BCP melt and shifts together with the modulus crossover.

6. Outlook

Findings for the lamellar PS-*b*-P2VP could be tested for other polymer systems. Possible variations with the same homopolymer blocks could be a variation of the morphology or the block number. Different polymer block combinations (i.e., PS-*b*-PI) could show the generality of the findings for PS-*b*-P2VP melts or show differences. As an example, results, such as the appearance of a maximum of ${}^3Q_0$ in the flow zone of BCP melts, are expected to be general properties. The ratio of the value of this peak to the one related to the polymer chain, might be different for other BCP systems due to a different χ for other polymer combinations. The temperature proximity of the maximum of the intrinsic nonlinearity and T_{ODT} could enable an approximate prediction of T_{ODT}. Despite for the BCP samples in this study, the determination of the nonlinearity by a variation of temperature was tested only on two homopolymer samples, and a comparative study to other measurement techniques could help to determine errors or differences to the other measurement techniques. The unusually high T_{ODT} of one of the PS-*b*-P2VP samples, which carries one DPE unit at its interface, may be further investigated for additional PS-*b*-P2VP samples but also other BCP combinations. The decoupling from the dependency on N may yield model systems, that might otherwise not be realized. From an application point of view, phase separation may be introduced in otherwise non-separating systems with only a minor change in the structure of the block copolymer chain.

Supporting Information

Supporting Information is available from the Wiley Online Library or from the author.

Acknowledgements

The authors gratefully thank the German Science Foundation (DFG) for financial support under the grant Wi 1911/22-2. The authors acknowledge Dr. Michael Pollard and Dr. Hyeong Yong Song for the proofreading and valuable comments on the manuscript.

Open access funding enabled and organized by Projekt DEAL.

Conflict of Interest

The authors declare no conflict of interest.

Data Availability Statement

The data that support the findings of this study are available from the corresponding author upon reasonable request.

Keywords

block copolymers, nonlinear oscillatory shear, phase separation, rheology

Received: December 15, 2023
Revised: June 7, 2024
Published online:

[1] T. P. Lodge, *Macromolecules* **2020**, *53*, 2.
[2] G. P. Baeza, *J. Polym. Sci.* **2021**, *59*, 2405.
[3] M. Robertson, Q. Zhou, C. Ye, Z. Qiang, *Macromol. Rapid Comm.* **2021**, *42*, 2100300.
[4] J. A. Yosick, A. Giacomin, P. Moldenaers, *J. Non-Newton. Fluid.* **1997**, *70*, 103.
[5] R. H. Ewoldt, P. Winter, J. Maxey, G. H. McKinley, *Rheol. Acta* **2010**, *49*, 191.
[6] G. Fleury, G. Schlatter, R. Muller, *Rheol. Acta* **2004**, *44*, 174.
[7] J. M. Brader, M. Siebenbürger, M. Ballauff, K. Reinheimer, M. Wilhelm, S. J. Frey, F. Weysser, M. Fuchs, *Phys. Rev. E* **2010**, *82*, 061401.
[8] K. S. Cho, K.-W. Song, G.-S. Chang, *J. Rheol.* **2010**, *54*, 27.
[9] I. Vittorias, D. Lilge, V. Baroso, M. Wilhelm, *Rheol. Acta* **2011**, *50*, 691.
[10] E. Helfand, D. S. Pearson, *J. Polym. Sci. Polym. Phys. Ed.* **1982**, *20*, 1249.
[11] D. S. Pearson, W. E. Rochefort, *J. Polym. Sci. Polym. Phys. Ed.* **1982**, *20*, 83.
[12] K. Hyun, M. Wilhelm, C. O. Klein, K. S. Cho, J. G. Nam, K. H. Ahn, S. J. Lee, R. H. Ewoldt, G. H. McKinley, *Prog. Polym. Sci.* **2011**, *36*, 1697.
[13] K. Hyun, M. Wilhelm, *Macromolecules* **2009**, *42*, 411.
[14] J. D. Ferry, *Viscoelastic properties of polymers*, 3rd ed., Wiley, New York **1980**.
[15] M. A. Cziep, M. Abbasi, M. Heck, L. Arens, M. Wilhelm, *Macromolecules* **2016**, *49*, 3566.
[16] M. Kempf, D. Ahirwal, M. Cziep, M. Wilhelm, *Macromolecules* **2013**, *46*, 4978.
[17] H. Y. Song, L. Faust, J. Son, M. Kim, S. J. Park, S.-k. Ahn, M. Wilhelm, K. Hyun, *Polymers-Basel* **2020**, *12*, 365.
[18] M. H. Wagner, V. H. Rolón-Garrido, K. Hyun, M. Wilhelm, *J. Rheol.* **2011**, *55*, 495.
[19] H. Y. Song, O. S. Nnyigide, R. Salehiyan, K. Hyun, *Polymer* **2016**, *104*, 268.
[20] V. H. Rolón-Garrido, *Rheol. Acta* **2014**, *53*, 663.
[21] M. H. Wagner, V. H. Rolón-Garrido, K. Hyun, M. Wilhelm, *J. Rheol.* **2011**, *55*, 495.

[22] K. Hyun, M. Wilhelm, *Macromolecules* **2009**, *42*, 411.
[23] T. Meins, N. Dingenouts, J. Kübel, M. Wilhelm, *Macromolecules* **2012**, *45*, 7206.
[24] T. Meins, K. Hyun, N. Dingenouts, M. Fotouhi Ardakani, B. Struth, M. Wilhelm, *Macromolecules* **2012**, *45*, 455.
[25] M. Langela, U. Wiesner, H. W. Spiess, M. Wilhelm, *Macromolecules* **2002**, *35*, 3198.
[26] M. Hoffmann, V. Hirschberg, N. Dingenouts, M. Wilhelm, *Macromolecules* **2023**, *56*, 10236.
[27] F. S. Bates, G. H. Fredrickson, *Annu. Rev. Phys. Chem.* **1990**, *41*, 525.
[28] V. Abetz, P. F. W. Simon, in *Block Copolymers I*, (Ed.: V. Abetz), vol. *189*, Springer-Verlag, Berlin/Heidelberg **2005**, pp. 125–212.
[29] I. W. Hamley, *J. Phys.-Condens. Mat.* **2001**, *13*, R643.
[30] M. W. Matsen, F. S. Bates, *Macromolecules* **1996**, *29*, 1091.
[31] L. Leibler, *Macromolecules* **1980**, *13*, 1602.
[32] L. Schneider, M. Heck, M. Wilhelm, M. Müller, *Macromolecules* **2018**, *51*, 4642.
[33] C. Liedel, C. W. Pester, M. Ruppel, V. S. Urban, A. Böker, *Macromol. Chem. Phys.* **2012**, *213*, 259.
[34] H. G. Schoberth, V. Olszowka, K. Schmidt, A. Böker, in *Complex Macromolecular Systems I*, (Eds.: A. H. E. Müller, H.-W. Schmidt), vol. *227*, Springer Berlin Heidelberg, Berlin, Heidelberg **2010**, pp. 1–31.
[35] C. W. Pester, C. Liedel, M. Ruppel, A. Böker, *Prog. Polym. Sci.* **2017**, *64*, 182.
[36] A. S. Merekalov, Y. I. Derikov, A. A. Ezhov, Y. A. Kriksin, I. Y. Erukhimovich, Y. V. Kudryavtsev, *Polymer* **2023**, *264*, 125544.
[37] J. M. J. LaFreniere, E. J. Roberge, J. M. Halpern, *J. Electrochem. Soc.* **2020**, *167*, 037556.
[38] A. S. Merekalov, Y. I. Derikov, V. V. Artemov, A. A. Ezhov, Y. V. Kudryavtsev, *Polymers* **2021**, *13*, 3959.
[39] B. McCulloch, G. Portale, W. Bras, J. A. Pople, A. Hexemer, R. A. Segalman, *Macromolecules* **2013**, *46*, 4462.
[40] M. Robertson, Q. Zhou, C. Ye, Z. Qiang, *Macromol. Rapid Comm.* **2021**, *42*, 2100300.
[41] M. Park, S. Kang, C. Nam, K. Narasimha, W. B. Lee, S.-J. Park, *ACS Appl. Mater. Inter.* **2022**, *14*, 8266.
[42] Z.-R. Chen, J. A. Kornfield, S. D. Smith, J. T. Grothaus, M. M. Satkowski, *Science* **1997**, *277*, 1248.
[43] M. Singh, A. Agrawal, W. Wu, A. Masud, E. Armijo, D. Gonzalez, S. Zhou, T. Terlier, C. Zhu, J. Strzalka, K. Matyjaszewski, M. Bockstaller, J. F. Douglas, A. Karim, *ACS Appl. Mater. Inter.* **2022**, *14*, 12824.
[44] W. Ding, J. Hanson, W. R. Burghardt, C. R. López-Barrón, M. L. Robertson, *Macromolecules* **2022**, *55*, 9465.
[45] J. Oh, M. Shin, I. S. Kim, H. S. Suh, Y. Kim, J. K. Kim, J. Bang, B. Yeom, J. G. Son, *ACS Nano* **2021**, *15*, 8549.
[46] M. Nébouy, L. Chazeau, J. Morthomas, C. Fusco, P. Dieudonné-George, G. P. Baeza, *J. Rheol.* **2021**, *65*, 405.
[47] V. Hirschberg, L. Faust, D. Rodrigue, M. Wilhelm, *Macromolecules* **2020**, *53*, 5572.
[48] M. Heck, L. Schneider, M. Müller, M. Wilhelm, *Macromol. Chem. Phys.* **2018**, *219*, 1700559.
[49] W. Zha, C. D. Han, D. H. Lee, S. H. Han, J. K. Kim, J. H. Kang, C. Park, *Macromolecules* **2007**, *40*, 2109.
[50] N. Hadjichristidis, H. Iatrou, S. Pispas, M. Pitsikalis, *J. Polym. Sci. Pol. Chem.* **2000**, *38*, 3211.
[51] N. Hadjichristidis, S. Pispas, G. Floudas, *Block copolymers: synthetic strategies, physical properties, and applications*, John Wiley & Sons, New York **2003**.
[52] A. K. Singh, A. Singh, *Comp. Mater. Sci.* **2023**, *226*, 112224.
[53] S. Lee, T. M. Gillard, F. S. Bates, *AIChE J.* **2013**, *59*, 3502.
[54] Q. Shi, J. Zou, C. Pan, Y. Fu, M. N. Supty, J. Sun, C. Yi, J. Hu, H. Tan, *e-Polymers* **2022**, *22*, 959.
[55] M. J. Rymaruk, C. T. O'Brien, C. György, B. Darmau, J. Jennings, O. O. Mykhaylyk, S. P. Armes, *Angew. Chem. Int. Ed.* **2021**, *60*, 12955.
[56] I. W. Hamley, V. Castelletto, *Prog. Polym. Sci.* **2004**, *29*, 909.
[57] M. Gopinadhan, C. O. Osuji, in *Encyclopedia of Polymeric Nanomaterials*, (Eds.: S. Kobayashi, K. Müllen), Springer Berlin Heidelberg, Berlin, Heidelberg **2014**, pp. 1–10.
[58] P. K. Singh, J. M. Soulages, R. H. Ewoldt, *J. Rheol.* **2018**, *62*, 277.
[59] H. Watanabe, T. Amemiya, T. Shimura, T. Kotaka, *Macromolecules* **1994**, *27*, 2336.
[60] N. Hadjichristidis, M. Pitsikalis, S. Pispas, H. Iatrou, *Chem. Rev.* **2001**, *101*, 3747.
[61] A. Munam, M. Gauthier, *J. Polym. Sci. Pol. Chem.* **2008**, *46*, 5742.
[62] H. Gausepohl, S. Oepen, K. Knoll, M. Schneider, G. McKee, W. Loth, *Des. Monomers Polym.* **2000**, *3*, 299.
[63] N. A. Bharadwaj, R. H. Ewoldt, *Rheol. Acta* **2015**, *54*, 223.
[64] H. Y. Song, R. Salehiyan, X. Li, S. H. Lee, K. Hyun, *Korea-Aust. Rheol. J.* **2017**, *29*, 281.
[65] M. Kempf, D. Ahirwal, M. Cziep, M. Wilhelm, *Macromolecules* **2013**, *46*, 4978.
[66] V. Hirschberg, M. Wilhelm, D. Rodrigue, *Polym. Test.* **2017**, *60*, 343.
[67] V. Hirschberg, F. Lacroix, M. Wilhelm, D. Rodrigue, *Mech. Mater.* **2019**, *137*, 103100.
[68] K. Reinheimer, M. Grosso, F. Hetzel, J. Kübel, M. Wilhelm, *J. Colloid Interf. Sci.* **2012**, *380*, 201.
[69] A. J. Patel, S. Narayanan, A. Sandy, S. G. J. Mochrie, B. A. Garetz, H. Watanabe, N. P. Balsara, *Phys. Rev. Lett.* **2006**, *96*, 257801.
[70] Y. Zhang, U. Wiesner, *J. Chem. Phys.* **1995**, *103*, 4784.
[71] M. L. Williams, R. F. Landel, J. D. Ferry, *J. Am. Chem. Soc.* **1955**, *77*, 3701.
[72] K. Hyun, S. H. Kim, K. H. Ahn, S. J. Lee, *J. Non-Newton. Fluid.* **2002**, *107*, 51.
[73] K. Hyun, M. Wilhelm, C. O. Klein, K. S. Cho, J. G. Nam, K. H. Ahn, S. J. Lee, R. H. Ewoldt, G. H. McKinley, *Prog. Polym. Sci.* **2011**, *36*, 1697.
[74] G. H. Fredrickson, R. G. Larson, *J. Chem. Phys.* **1987**, *86*, 1553.